Figure 1 Structural characterizations of the $BiFeO_3$. (a) XRD patterns. (b) EDS spectrum. (c) Fe 2*p* core level XPS spectrum. (d) Bi 4*f* core level XPS spectrum.

The XRD patterns are shown in Figure 1a. All the diffraction peaks can be assigned to a pure rhombohedral phase of $BiFeO_3$ with a space group of *R*3*c* and a point group 3*m* (JCPDS Card no. 86-1518). In Figure 1b, the energy dispersive X-ray spectroscopy (EDS) shows the existence of Bi (8.27%), Fe (7.37%), O (67.74%), Al (15.40%) and Au (1.25%), where Al and Au come from the sample holder and the sputtered Au coating on the powder sample, respectively. XPS was used to investigate the oxidation states of the Bi and Fe elements in $BiFeO_3$. Figure 1c is the high resolution XPS spectrum of Fe 2*p*, showing the binding energy of 711.02 eV for Fe $2p_{3/2}$ and 725.27 eV for Fe $2p_{1/2}$ with a spin orbit splitting of 14.25 eV, which were characteristic for Fe^{3+}.[15] The high resolution XPS spectrum of Bi 4f (Figure 1d) shows two peaks around 159.22 and 164.47 eV, corresponding to Bi $4f_{7/2}$ and Bi $4f_{5/2}$ of the Bi^{3+} state, respectively.[16] Figure S1a is a schematic diagram displaying the circuit for the *P-E* hysteresis loop measurement. A well-developed *P-E* loop can be observed in Figure S1b, indicating the ferroelectric nature of $BiFeO_3$. The saturation polarization is achieved at an applied electric field of 5.0 kV·mm⁻¹.
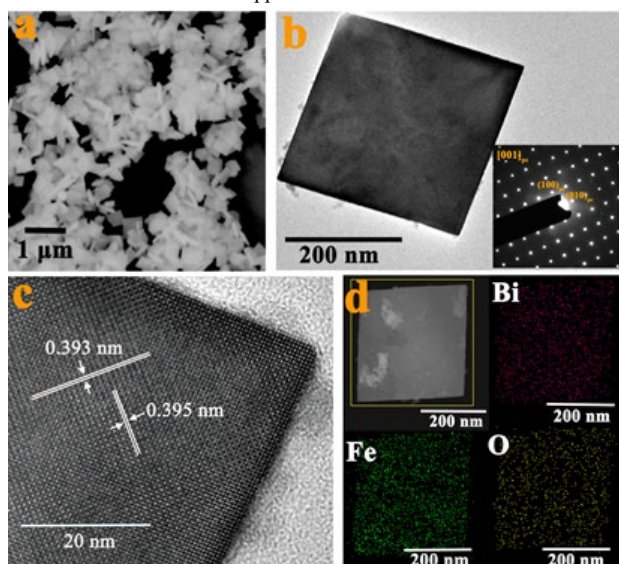

Figure 2 Morphology characterizations of the $BiFeO_3$ nanosheets. (a) SEM image. (b) TEM bright-field image with electron diffraction pattern as inset. (c) High resolution TEM image. (d) Scanning TEM image together with the corresponding elemental mapping.

The SEM and TEM micrographs are shown in Figure 2a and 2b, respectively. The as-prepared $BiFeO_3$ catalyst possesses a morphology of square nanosheet with an average size of ~380 nm. Size distribution of the $BiFeO_3$ nanosheets is shown in Figure S2. The selected area electron diffraction pattern (SAED) is shown in the inset of Figure 2b, indicating the normal direction of $BiFeO_3$ nanosheet being along [001]pc (The subscript "pc" refers to a "pseudo-cubic" structure adopted here for easy indexing). The high resolution TEM image (Figure 2c) of the nanosheet shows two characteristic lattice spacings, both around 0.395 nm, which agree well the *d*-spacings of the $(100)_{pc}$ and $(010)_{pc}$ planes of $BiFeO_3$. Furthermore, the scanning TEM image and the associated elemental mappings of Bi, Fe and O (Figure 2d) show uniform distributions of these elements.
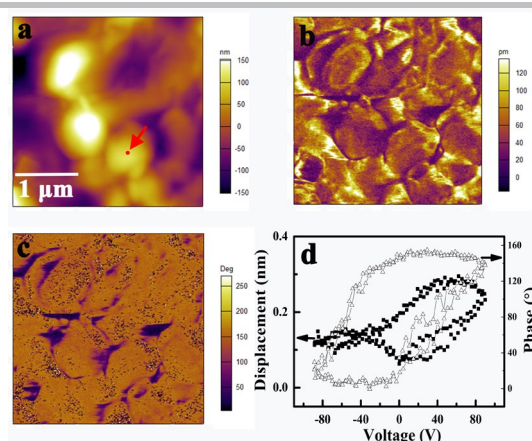

Figure 3 PFM of $BiFeO_3$ nanosheets. (a) Morphology image. (b) Amplitude image. (c) Phase image. (d) Hysteresis loop.

The piezoelectric property of $BiFeO_3$ nanosheets was characterized by a piezoresponse force microscope (PFM), using dual alternating current resonance tracking (DART) modes in order to expel the displacement contribution from electrostatic interaction and topographical crosstalk in mapping the local electromechanical properties. The topographic, vertical piezoresponse amplitude, and phase images of the $BiFeO_3$ nanosheets are shown in Figure 3a-3c, respectively. The $BiFeO_3$ nanosheets can be clearly detected in the topographic image with clear contrasts in the amplitude and phase images. A localized hysteresis loop is observed (Figure 3d), where the phase angle changes by 160° under the reversal of 90 V direct current (DC) bias field, confirming the piezoelectricity of the $BiFeO_3$ nanosheets.
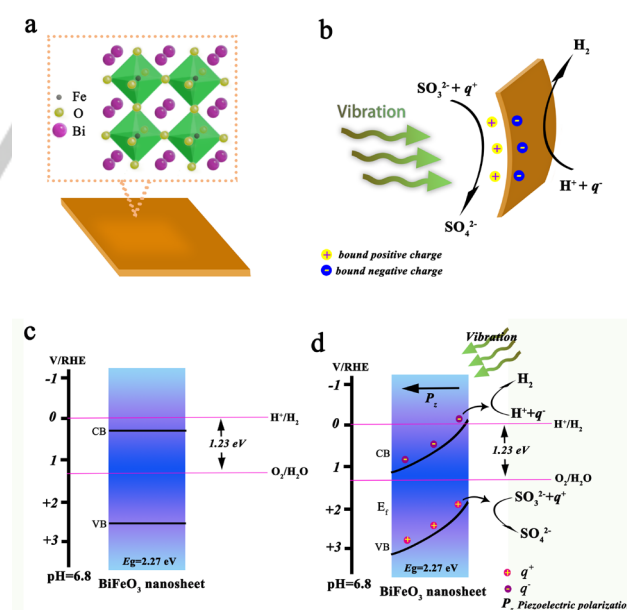

Figure 4 Schematic illustration of the piezo-catalysis mechanism and tilting of energy bands. (a) Atomic structure of $BiFeO_3$. (b) The generation of piezoelectric surface charges under mechanical vibration and the participation of piezo-catalytic hydrogen evolution reaction. (c) Energy band diagram without mechanical vibration. (d) Tilting of energy bands under the strong piezoelectric field induced by mechanical vibration and the accompanied redox reactions.

The basic principle of piezo-catalysis is shown in Figure 4a-b. $BiFeO_3$ nanosheet with a rhombohedral phase is piezoelectric due to the non-central symmetry of its 3*m* point group. When subjected to